International Journal of Solids and Structures 51 (2014) 1103–1114

Contents lists available at ScienceDirect

International Journal of Solids and Structures

journal homepage: www.elsevier.com/locate/ijsolstr

Non-coaxiality of strain increment and stress directions in cross-anisotropic sand

Nina M. Rodriguez [a], Poul V. Lade [b,*]

[a] Department of the Navy, Naval Sea Systems Command 05C, Washington Navy Yard, Washington, DC 20376, USA
[b] Department of Civil Engineering, The Catholic University of America, Washington, DC 20064, USA

ARTICLE INFO

Article history:
Received 4 June 2013
Received in revised form 25 November 2013
Available online 16 December 2013

Keywords:
Cross-anisotropy
Non-coaxiality
Sand
Three-dimensional
Torsion shear

ABSTRACT

An experimental program was carried out in a recently developed torsion shear apparatus to study the non-coaxiality of strain increment and stress directions in cross-anisotropic deposits of Fine Nevada sand. Forty-four drained torsion shear tests were performed at constant mean confining stress, σ_m, constant intermediate principal stress ratios, as indicated by $b = (\sigma_2 - \sigma_3)/(\sigma_1 - \sigma_3)$, and constant principal stress directions, α. The experiments were performed on large hollow cylinder specimens deposited by dry pluviation and tested in an automated torsion shear apparatus. The specimens had height of 40 cm, and average diameter of 20 cm, and wall thickness of 2 cm. The stress–strain behavior of Fine Nevada sand is presented for discrete combinations of constant principal stress direction, α, and intermediate principal stress. The effects of these two variables on the non-coaxiality are presented. The experiments show that the directions of the strain increments do not in general coincide with the directions of stresses, and there is a switch from one to the other side between the two quantities.

1. Introduction

The issue of the direction of the major principal strain increment relative to the direction of the major principal stress has interest for modeling of these quantities using elasticity and plasticity theories. For cross-anisotropic materials these directions are not expected to coincide. A detailed experimental investigation was performed for cross-anisotropic sand deposits in a hollow cylinder torsion shear apparatus. The notation for the physical quantities used here is given in Table 1. A series of torsion shear experiments was performed on large hollow cylinder specimens of Fine Nevada sand with constant principal stress directions relative to vertical, α, varying between 0° and 90° and with the intermediate principal stress, σ_2, varying from σ_3 to σ_1 as indicated by $b = (\sigma_2 - \sigma_3)/(\sigma_1 - \sigma_3)$. The Fine Nevada sand was deposited by dry pluviation, thus producing a sand fabric with horizontal bedding planes and cross-anisotropic characteristics. The various stress conditions were achieved by varying the pressures inside and outside the hollow cylinder specimen relative to the shear stress and the vertical deviator stress according to a pre-calculated pattern. All stresses and all strains were determined from careful measurements so that analysis of the soil behavior could be made reliably. The soil behavior was determined for a pattern of combinations of α varying with increments of 22.5° from 0° to 90° and b varying with increments of 0.25 from 0.0 to 1.0. Thus, 25 test locations were established, but many tests were repeated to study the consistency of the results. The measured stress–strain behavior is presented for 15 tests in which the major principal stress was not aligned with or perpendicular to the bedding planes. The results show that strain increment directions are generally not coinciding with the major principal stress directions. When the major principal stress forms angles greater than approximately 45° with the bedding planes, the major principal strain increment directions are closer to the bedding plane direction. However, a switch occurs such that when the major principal stress direction forms more shallow angles below 45° with the bedding planes, the direction of the major principal strain increment is steeper than the direction of the major principal stress. All tests except those with $b = 0.0$ resulted in shear bands, after which strains are not uniform anymore.

2. Previous studies

A significant aspect of soil behavior, which may be modeled by hardening plasticity theory, is that relating to coincidence in physical space of principal strain increments with principal stresses and the influence of anisotropy on this behavior. The stress–strain behavior of sands measured in torsion shear tests has previously been analyzed in terms of the directions of major principal strain increment and major principal stress during

* Corresponding author. Tel.: +1 202 319 6942; fax: +1 202 319 6677.
E-mail addresses: nina.m.rodriguez1@navy.mil (N.M. Rodriguez), Lade@cua.edu (P.V. Lade).

0020-7683/$ - see front matter © 2013 Elsevier Ltd. All rights reserved.
http://dx.doi.org/10.1016/j.ijsolstr.2013.12.003

Table 1
Notation for physical quantities.

Symbol	Physical quantity
b	$=(\sigma_2-\sigma_3)/(\sigma_1-\sigma_3)$ = relative magnitude of the intermediate principal stress
D_{50}	Mean diameter of sand grains
e	Void ratio
F_v	Vertical load on hollow cylinder specimen
h	Height of hollow cylinder specimen
LVDT	Linear variable differential transducer
p_0, p_i	Outside and inside pressures on hollow cylinder specimen
R	σ_1/σ_3
R_0, R_i	Outside and inside radii of hollow cylinder specimen
T	Torque applied to hollow cylinder specimen
α	Inclination of major principal stress to vertical
β_R	Non-uniformity index = $(R_{max}-R_{min})/R_{avg}$
$\gamma_{z\theta}$	$=2\cdot\varepsilon_{z\theta}$ = engineering shear strain
Δ	$=(\xi-\alpha)$ = angle between directions of major principal strain increment and major principal stress
ΔI_{vol}	Volume change of inner cell
ΔV	Volume change of specimen
$\Delta\theta$	Twist angle of hollow cylinder specimen
ε_z, ε_θ, ε_r	Vertical, tangential and radial normal strains
ε_1	Major principal strain
$\varepsilon_{z\theta}$	Shear strain
ξ	Inclination of major principal strain increment to vertical
σ_v, σ_θ, σ_r	Effective vertical, tangential, and radial stresses on hollow cylinder specimen
σ_1, σ_2, σ_3	Effective major, intermediate, and minor principal stresses
σ_m	Effective mean normal stress
$\tau_{z\theta}$	Torsional shear stress

rotation of principal stress axes in physical space (e.g. Lade 1975, 1976; Hight et al., 1983; Ishihara and Towhata, 1983; Tatsuoka et al., 1986; Symes et al., 1984, 1988; Pradhan et al., 1988; Vaid et al., 1990; Vaid and Sayao, 1995; Saada et al., 1999; Zdravkovic and Jardine, 2000; Sivathayalan and Vaid, 2002; Chaudhary and Kuwano, 2003; Yang et al., 2007; Lade et al., 2008, 2009). Similar testing and analyses have also been performed on clay (e.g. Broms and Casbarian, 1965; Saada and Baah, 1967; Hicher and Lade, 1987; Saada et al., 1994; Frydman et al., 1995; Hong and Lade, 1989a and b; Lade and Kirkgard, 2000; Nishimura et al., 2007). Lade et al., (2009) showed that modeling the observed behavior by an isotropic, plastic hardening soil implies that the two sets of directions coincide during stress rotation, but loading along the principal axes of an anisotropic material will also result in coincidence of principal stress axes with principal strain increment axes. The influence of cross-anisotropy, as is most often found in naturally deposited soils, may not be present in slope talus, sand dunes, or for fluvial or marine sands that have been mobile. However, the effect of cross-anisotropy on the soil behavior has drawn most attention and has been at the root of the use of torsion shear tests with stress rotation in many studies exemplified by those listed above.

3. Torsion shear tests on hollow cylinder specimens

Torsion shear tests performed on hollow cylinder specimens are conducted in an apparatus as shown in Fig. 1. These tests are suitable for investigating the effects of principal stress directions on the behavior of soil, because in these tests the bedding planes remain horizontal and the principal stresses can be rotated relative to the bedding planes. In addition, there are only minor effects of imposed non-uniform stress conditions if the specimen is sufficiently tall (Lade, 1981). The state of stress in the hollow cylinder specimen is shown in Fig. 2. In these experiments the direction of the major principal stress may be changed relative to the cross-anisotropic deposit created by dry pluviation. This allows studying the direction of major principal strain increment relative

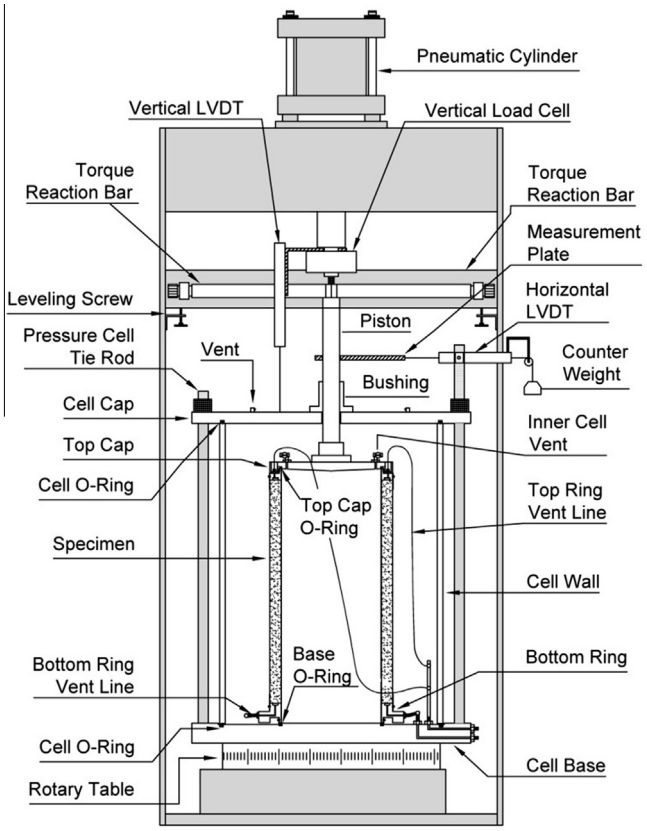

Fig. 1. Schematic drawing of torsion shear apparatus.

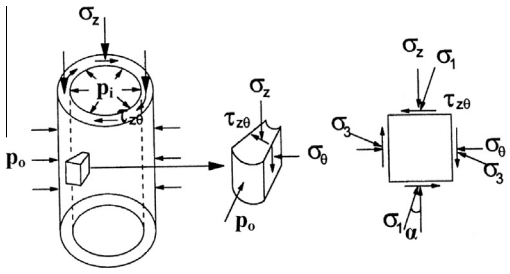

Fig. 2. Stress state in wall of hollow cylinder specimen during torsion shear test.

to the direction of the major principal stress in cross-anisotropic sand deposits. The strength results of such torsion shear tests on dense, Fine Nevada sand were presented by Lade et al. (2013), and the non-coaxiality of strain increment and stress directions are presented and analyzed here.

3.1. Sand tested

All torsion shear tests were performed on Fine Nevada sand, which is composed of subangular to subrounded grains consisting mainly of quartz (98%). The properties of this sand are as follows: Mean diameter, D_{50} = 0.23 mm; coefficient of uniformity, 2.08; coefficient of curvature, 1.05; specific gravity, 2.65; maximum void ratio, 0.771; and minimum void ratio, 0.507.

3.2. Preparation of hollow cylinder specimens

The boundaries of the hollow cylinder specimen consisted of custom molded inner and outer latex rubber membranes attached to stainless steel end rings. Hollow cylinder specimens with hori-

zontal bedding planes were prepared using the pluviation and saturation techniques described by Lade et al. (2013). All specimens had inner and outer diameters of 18.0 cm and 22.0 cm, respectively, and the wall thickness was therefore 2.0 cm. The height of the hollow cylinder was 40 cm. These dimensions are in agreement with those recommended by Sayao and Vaid (1991). They proposed that the wall thickness should be in the order of 2.0–2.6 cm to include a sufficiently large number of sand grains across the wall to ensure uniform sand density and to minimize the significance of membrane penetration effects on the measured volume changes. They also suggested that a satisfactory geometry of the hollow cylinder specimen with regard to non-uniformity and experimental control would be obtained if R_i/R_o were within 0.65 to 0.82. The present hollow cylinder has $R_i/R_o = 0.82$. To reduce the influence of radial friction, the height was recommended be such that $H/2R_o = 1.8–2.2$. The present apparatus employs $H/2R_o = 40/22$ cm = 1.82. However, actual experiments on sand show that a height of 25 cm is sufficient to obtain acceptable results (Lade, 1981; Lade et al., 2008). Thus, the specimen dimensions are favorable to producing satisfactory experimental results.

Molds or forming jackets were used to hold the inner and outer latex rubber membranes while pluviating the sand. Two factors affect the void ratio when pouring the sand: The drop height and the rate of sand pluviation. In order to ensure the same void ratio for each specimen, the sand was poured into a funnel with a small tube inside the mouth of the funnel ensuring a constant flow rate of sand. It was determined empirically that a drop height of 35 cm at the employed flow rate would create the desired void ratio. As the sand was deposited, the funnel was carefully raised to ensure a drop height of 35 cm and even bedding planes in the assembled mold. A void ratio, $e = 0.53$ was targeted for each specimen. This corresponds to a relative density of 91% for the Fine Nevada sand.

Fig. 1 shows that the base plate of the torsion shear apparatus was rigidly attached to a rotary table, whose rotation was driven by a gear motor with constant rate and resisted by a piston protruding through the top plate. The hollow cylinder specimen was sitting between a base ring and a top ring which in turn were attached to the base plate and the piston. Thus, the hollow cylinder specimen was exposed to the torque between the base plate and the piston.

In torsion shear tests with the same inside and outside pressures, the value of $b = (\sigma_2 - \sigma_3)/(\sigma_1 - \sigma_3)$ is tied to the inclination, α, of the major principal stress such that $b = \sin^2\alpha$. In the torsion shear apparatus employed here different pressures could be applied to the inner and outer cells, thus making it possible to separate the major principal stress inclination, α, from the value of b. The torque was measured at the piston and it was used to calculate and control the vertical load and the inside and outside pressures in such a way as to follow a prescribed stress path. The pressures and forces in the torsion shear apparatus were computer controlled. The necessary equations were installed in the computer and for each prescribed increment in torque the vertical load and the inner and outside pressures were updated and applied. Since deformations were also measured, it was possible to calculate the actual pressures and shear stresses and apply them in real time. Further details regarding the specimen construction and saturation of the inner cell are given by Lade et al. (2013).

3.3. Calculation of stresses and strains

Representative average stresses and strains for thin-walled cylinders were determined from the following expressions:

Vertical stress:

$$\sigma_z = \frac{F_v}{\pi(R_0^2 - R_i^2)} + \frac{R_0^2 \cdot p_0 - R_i^2 \cdot p_i}{R_0^2 - R_i^2} \tag{1}$$

in which F_v is the vertical load, p_0 and p_i are the outside and the inside pressures, and R_0 and R_i are the outside and the inside radii of the hollow cylinder.

Radial stress:

$$\sigma_r = \frac{R_0 \cdot p_0 + R_i \cdot p_i}{R_0 + R_i} \tag{2}$$

Tangential stress:

$$\sigma_\theta = \frac{R_0 \cdot p_0 - R_i \cdot p_i}{R_i - R_0} \tag{3}$$

Shear stress:

$$\tau_{z\theta} = \frac{3 \cdot T}{2\pi(R_0^3 - R_i^3)} \tag{4}$$

in which T is the torque applied to twist the hollow cylinder.

Corrections were applied to the data after the tests were performed due to vertical piston uplift, membrane strength, etc.

Vertical strain:

$$\varepsilon_z = \frac{\Delta h}{h_0} \tag{5}$$

in which h_0 is the initial height and Δh is the change in height of the hollow cylinder specimen.Radial strain:

$$\varepsilon_r = -\frac{\Delta R_0 - \Delta R_i}{R_0 - R_i} \tag{6}$$

Tangential strain:

$$\varepsilon_\theta = -\frac{\Delta R_0 + \Delta R_i}{R_0 + R_i} \tag{7}$$

in which ΔR_0 and ΔR_i are the changes in outside and inside radii determined from the following expressions (see Lade et al., 2009):

$$\Delta R_0 = \sqrt{\frac{\pi(R_0^2 h_0) + \Delta I_{vol} + \Delta V}{\pi h}} - R_0 \tag{8}$$

$$\Delta R_i = \sqrt{\frac{\pi(R_i^2 h_0) + \Delta I_{vol}}{\pi h}} - R_i \tag{9}$$

in which ΔI_{vol} and ΔV are the changes in volumes of the inner cell and the specimen, respectively.

Shear strain:

$$\varepsilon_{z\theta} = \frac{\Delta\theta\left(R_0^3 - R_i^3\right)}{3h\left(R_0^2 - R_i^2\right)} \tag{10}$$

in which:

$$\Delta\theta = \frac{\Delta H_{LVDT}}{r_{measurementplate}} \tag{11}$$

where ΔH_{LVDT} is the recorded change in the horizontal LVDT reading and $r_{measurementplate}$ is the distance from the center to the radio wire cord of the pie-shaped measurement plate.

It should be pointed out that no unloading and reloading cycles were performed to study yield surfaces, both primary and kinematic, which require resolution of strains to better than 0.1%, such as done by e.g. Shibuya et al. (2003) in hollow cylinder tests and by Kuwano and Jardine (2007) in triaxial tests.

3.4. Stress non-uniformity

To study stress concentrations across the cylinder wall, Sayao and Vaid (1991) assumed the wall to be thick compared with the cylinder radius ($t/R > 0.1$) and the influence of the material's consti-

tutive behavior on the stresses therefore becomes more important. The vertical stress is not affected by the material behavior and is obtained from equilibrium alone, as given in Eq. (1).

Sayao and Vaid (1991) produced the following expressions for the horizontal normal stresses and the shear stress in the hollow cylinder:

$$\sigma_r = \frac{R_0^2 \cdot p_0 - R_i^2 \cdot p_i}{R_0^2 - R_i^2} - \frac{2(p_0 - p_i) \cdot R_0^2 \cdot R_i^2 \cdot \ell n(R_0/R_i)}{R_0^2 - R_i^2} \tag{12}$$

$$\sigma_\theta = \frac{R_0^2 \cdot p_0 - R_i^2 \cdot p_i}{R_0^2 - R_i^2} + \frac{2(p_0 - p_i) \cdot R_0^2 \cdot R_i^2 \cdot \ell n(R_0/R_i)}{R_0^2 - R_i^2} \tag{13}$$

$$\tau_{z\theta} = \frac{4 \cdot T \cdot (R_0^3 - R_i^3)}{3\pi(R_0^4 - R_i^4)(R_0^2 - R_i^2)} \tag{14}$$

Using these expressions the principal stresses can be determined everywhere across the wall and for any inclination of the major principal stress relative to vertical. Sayao and Vaid (1991) then devised an index of stress non-uniformity in terms of the principal stress ratio, $R = \sigma_1/\sigma_3$, as follows:

$$\beta_R = \frac{R_{max} - R_{min}}{R_{avg}} \tag{15}$$

As an example, Fig. 3 shows the variation of the stress non-uniformity index across the wall in the hollow cylinder specimen (inner radius = 5.0 cm, outer radius = 7.5 cm) employed by Sayao and Vaid (1991) for an average stress ratio of $R = 3.0$. Other dimensions will produce different but similar stress non-uniformity indices. It is seen from the diagram in Fig. 3 that the index is zero for conventional triaxial compression ($b = 0.0$) with a vertical major principal stress ($\alpha = 0°$), while the conventional triaxial extension conditions ($b = 1.0$) and a vertical major principal stress ($\alpha = 0°$) exhibits the highest stress concentration index. For horizontal major principal stresses ($\alpha = 90°$), the highest index is obtained for triaxial compression ($b = 0.0$) and the lowest index is produced for triaxial extension ($b = 1.0$). The effects of these stress non-uniformities in the torsional hollow cylinder specimens were studied and reported by Lade and Rodriguez (2013).

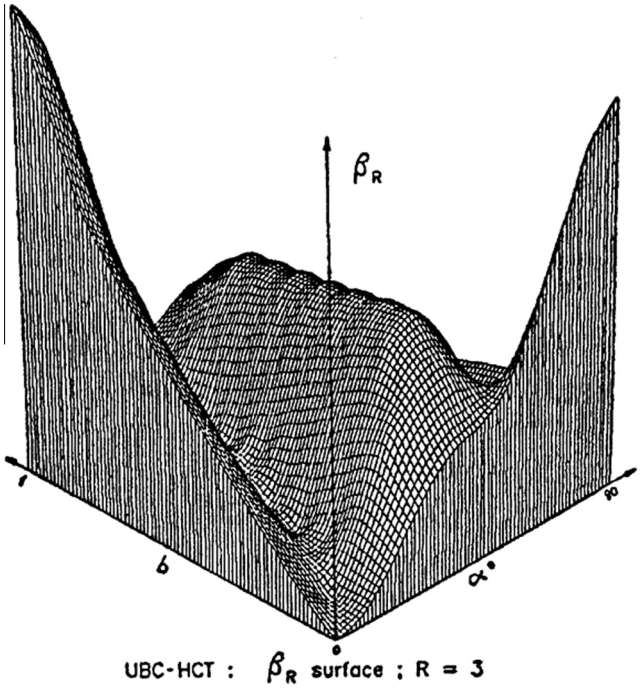

Fig. 3. Variation of stress non-uniformity index across the wall of hollow cylinder specimens with dimensions employed in torsion shear tests performed at University of British Columbia by Sayao and Vaid (1991).

3.5. Instrumentation and control of experiments

The physical quantities of loads, pressures and deformations were measured by load cells, pressure transducers, LVDTs, and volume change devices. Fig. 1 shows that a load cell was placed between the vertical piston and an air pressure cylinder located at the top of the rigid loading frame. To measure the shear stresses, a crossbar assembly was rigidly attached to the piston and two torque arms with load cells were connected to a back plate of the rigid frame. Springs were placed between the torque load cells and the rigid body frame to allow for compression and extension of the arms. A vertical LVDT was fastened to the piston to measure the axial deformation of the specimen. The shear deformation was measured at a constant distance from the center of the piston by a horizontal LVDT attached to the top plate of the chamber. The volume changes of the specimen and the inner cell were measured and allowed determination of the normal strains in the horizontal directions.

A main panel board applied pressures and measured the volume changes of the specimen during shearing. The inner and outer pressures and the back pressure applied to the hollow cylinder specimen were measured by pressure transducers and displayed on pressure gages. These pressures could be applied both manually by a pressure regulator and automatically by the computer when the LabView program was turned on. An on/off switch valve allowed for the switch between automatic and manual control. The constant back pressure was applied with a manual regulator and indicated on a pressure gage. The vertical load could also be applied both manually and automatically to the specimen. Lower and upper air pressure lines were connected to the vertical air pressure cylinder allowing for both compression and extension tests to be performed. Differential pressure transducers were employed to measure the volume changes of the inner cell and the specimen, and together with the LVDT measurements, they provided sufficient information for calculation of the current strains in the hollow cylinder specimen. This allowed calculation of simultaneous stresses and strains, given by the formulas in Section 3.3, for accurate control of the experiment.

The internal and external pressure transducers, inner cell and specimen volume change transducers, vertical load cell, the two torque load cells and horizontal LVDT and vertical LVDT were all connected to a data acquisition unit and displayed in LabView. This computer program reads the electrical signals from the measurement devices and through calibration inputs in the program, the signals were converted to pressures, loads and distances. These were used to compare with the intended quantities and then used for control of b-values, α-values and mean normal stress σ_m, as initially input to the program. Once a set of measurements was acquired by the LabView program, the internal and external pressures and the vertical load applied to the hollow cylinder specimen were changed to ensure the designated b-value and α-value were applied to the specimen while keeping the mean normal stress constant. The applied pressures and loads were recorded, as well as the inner volume change, specimen volume change, horizontal LVDT and vertical LVDT readings. These readings provided the necessary data to study the behavior of the sand under different stress paths.

3.6. Experimental procedure and program

A series of 44 drained tests was performed in this experimental program to study the behavior of dense, Fine Nevada sand while

keeping b, α, and σ_m constant. The specimens were saturated by the CO_2-method (Lade and Duncan, 1973). Skempton's B-value was determined and all specimens showed B-values above 0.94, which indicates sufficient degrees of saturation for drained tests on dense sand. Once ready to begin testing, the specimens underwent isotropic consolidation in increments in effective confining pressure of 6.9 kPa from 48.3 kPa to 101 kPa. This initial isotropic consolidation may have affected the anisotropy of the specimens with the result that they may have become slightly more isotropic in behavior, as observed by Lade and Abelev (2005) for triaxial specimens and by Shibuya et al. (2003) for torsion shear hollow cylinder specimens.

Shearing began for all specimens at the initial isotropic effective confining pressure of 101 kPa. Depending on the stress path indicated for the particular test, the vertical force was either in compression or tension for constant mean stress, b-value and α-value. Note that the vertical stress was always in compression, even when the vertical force applied through the central shaft was in tension, because it was counteracted by the confining pressures. The inner and outer confining pressures either increased or decreased from the initial value of 101 kPa. All efforts were made to stay as close to the targeted b- and α-values as possible during testing.

To establish the conditions for all combinations of intermediate principal stress, as expressed by $b = (\sigma_2 - \sigma_3)/(\sigma_1 - \sigma_3)$, and σ_1-directions from $\alpha = 0°$ to $\alpha = 90°$, experiments were performed at each of the 25 intersection points of $b = 0.0$, 0.25, 0.50, 0.75, and 1.00 and $\alpha = 0°$, 22.5°, 45.0°, 67.5°, and 90.0°. For each of these experiments the stress–strain and volume change and strength behavior were determined.

These experiments were performed while maintaining the mean normal stress constant at 101 kPa. The tests were conducted by rotating the rotary table thereby increasing the torque and then adjusting all other quantities to the torque to follow the desired stress path. Each experiment would typically take 2–3 h. However, effects of loading rate are negligible at low stresses because only very small amounts of crushing (which is responsible for time effects in granular materials) occur at low stresses.

Tests without stress rotation and with $\alpha = 0°$ and $\alpha = 90°$ do not require torque, and they were stress controlled tests. For these tests, the major principal stress and the major principal strain increments coincide in vertical or horizontal directions. The results of these tests were compared with true triaxial tests by Lade and Rodriguez (2013) and these results will not be discussed further here.

4. Stress–strain and volume change behavior

The stress–strain and volume change behavior are shown in Figs. 4–6 for torsion shear tests with $\alpha = 22.5°$, 45°, and 67.5° and for all b-values from 0 to 1. The results are presented as stress ratio, σ_1/σ_3, versus the major principal strain, ε_1. These values are calculated from the measured normal and shear stresses and normal and shear strains. The results in Figs. 4(a), 5(a), and 6(a) clearly indicate that the initial slopes of the $\sigma_1/\sigma_3 - \varepsilon_1$ relations increase, the strains-to-failure decrease, and the strengths, as indicated by the maximum values of σ_1/σ_3 (or the friction angles), increase with increasing b-value, except for $b = 1$, where these quantities decrease. The arrows indicate the points of failure. The volume change curves in Figs. 4(b), 5(b), and 6(b) show that the rate of dilation, defined as $d\varepsilon_v/d\varepsilon_1$, increases with increasing b-values. Thus, with respect to these quantities the variation in behavior with b-values is very similar to those observed in true triaxial tests on sands (Lade and Duncan, 1973; Wang and Lade, 2001; Abelev and Lade, 2003).

The strength results of the torsion shear tests on Fine Nevada sand were presented and discussed by Lade et al. (2013).

5. Analyses of strain increment and stress directions

The directions of total strain increments and stress directions for the tests with $\alpha = 22.5°$, 45°, and 67.5° and for all b-values from 0 to 1 were analyzed using Mohr circles for strain increments and stresses throughout each test. Total strain increments were analyzed, i.e. the strain increments consisted of both elastic and plastic strain increments. In previous publications (e.g. Lade et al., 2009) the directions of major principal strain increments in physical space were superimposed on diagrams of directions of major principal effective stress so the progressive alignment (or lack thereof) could be seen. To show more directly the deviations between these two directions in this presentation, the directions are shown as angles (α = major principal effective stress direction relative to vertical and ξ = major principal strain increment direction relative to vertical)) versus engineering (torsional) shear strain ($\gamma_{z\theta} = 2 \cdot \varepsilon_{z\theta}$). As is seen in Figs. 7–11, the initial response which is dominated by elastic strains creates an initial deviation of major strain increment direction (open circles) from the major stress direction (open squares) due to the cross-anisotropic behavior of the sand. As more stress is applied, the specimen moves into the plastic range of the stress–strain curve, and the major strain increment directions tends towards the major principal stress directions. The largest deviation is seen in the tests with $\alpha = 22.5°$. Since there are no external shear strains in the tests with $\alpha = 0°$ and $\alpha = 90°$, their directions coincide with the directions of the major principal stress and they are not plotted on the diagrams. Points are plotted up to failure represented by shear banding in all test except those with $b = 0.0$. Strains after failure are not considered as they are highly non-uniform due to development of shear bands. Not all tests followed the desired stress paths in terms of the α- and b-values, but representative results of tests that had the correct stress path have been presented in Figs. 7–11.

As seen in Fig. 7 for tests with $b = 0$, test # TS 3 starts out having a significantly higher ξ-direction than α-direction, which is reasonably constant at 22.5°. As the specimen is sheared, the ξ-direction approaches the α-direction. The ξ-direction becomes constant near engineering shear strains of $\gamma_{z\theta} = 1.5\%$, and the deviation from the α-direction remains constant at approximately 6°. In test # TS 14 with $\alpha = 67.5°$, a small deviation develops between the two directions until about $\gamma_{z\theta} = 0.5\%$ after which the ξ-direction asymptotically approaches the α-direction. In test # TS 31 the two directions start out at 45°, but the ξ-direction begins to deviate from the α-direction at around $\gamma_{z\theta} = 0.5\%$ and the two directions remain apart at around 3° for the rest of the test.

Similar to the results in Fig. 7, tests with higher b-values in Figs. 8–11 show domination of the elastic behavior at the beginning of the tests. While smaller plastic strains occur from the beginning of shearing, the strains include larger plastic components as failure is approached, and the major principal strain increment directions tend to approach the major principal stress directions, and the experiments with $\alpha = 67.5°$ show slightly lower ξ-directions. Although not large, the relatively largest variation occurs at $\alpha = 22.5°$. At $\alpha = 45°$ the major principal strain increment directions are closest to the principal stress directions throughout the entire experiments on the hollow cylinder specimens. Tests with $b = 1.0$, shown in Fig. 11, exhibit the largest variation near the beginning of the test, where the elastic strains dominate.

Fig. 12 summarizes the deviations of principal strain increment directions and principal stress directions at failure for all torsion shear experiments. On the average these deviations vary between $\Delta = \xi - \alpha = +3.6°$ at $\alpha = 22.5°$ over $\Delta = \xi - \alpha = +1.1°$ at $\alpha = 45°$ to $\Delta = \xi - \alpha = -5.5°$ at $\alpha = 67.5°$. While there is some scatter in the results for each of the principal stress inclinations, i.e. the standard deviations on the Δ-values are ±2.3°, ±1.4°, and ±3.1°, respectively,

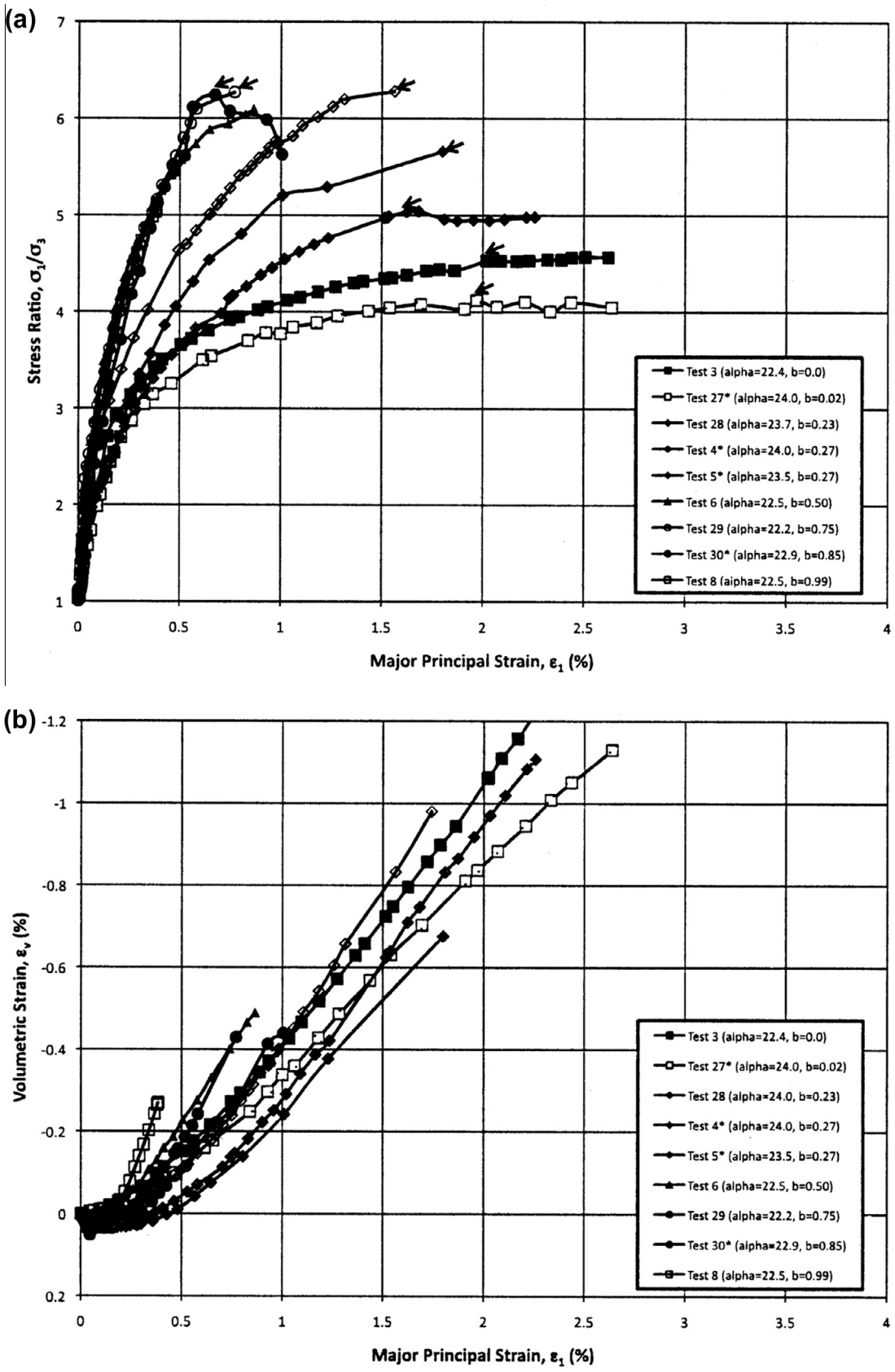

Fig. 4. (a) Stress–strain and (b) volume change relations for torsion shear test with $\alpha = 22.5°$ on hollow cylinder specimens of dense Nevada sand.

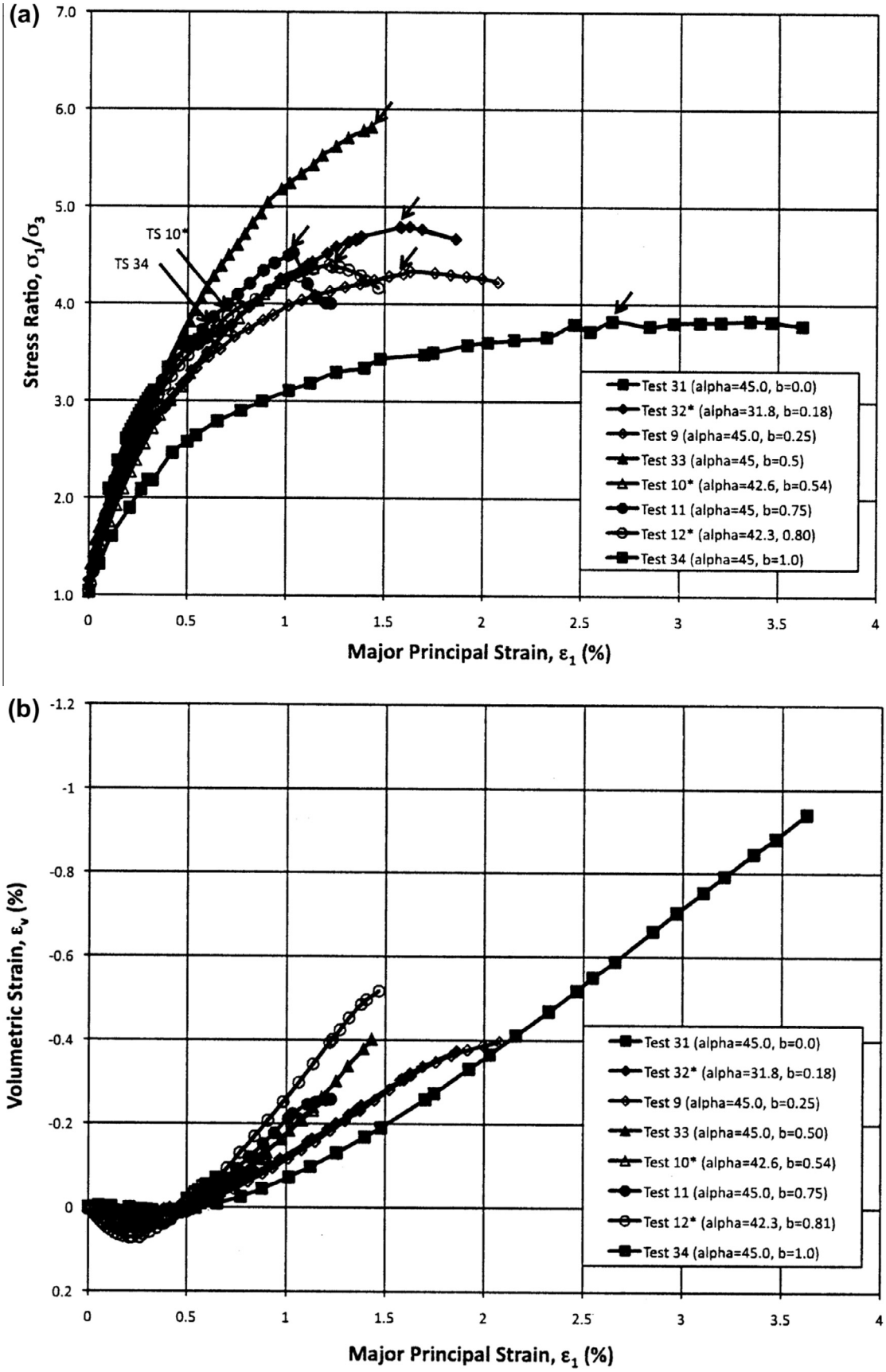

Fig. 5. (a) Stress–strain and (b) volume change relations for torsion shear test with $\alpha = 45^\circ$ on hollow cylinder specimens of dense Nevada sand.

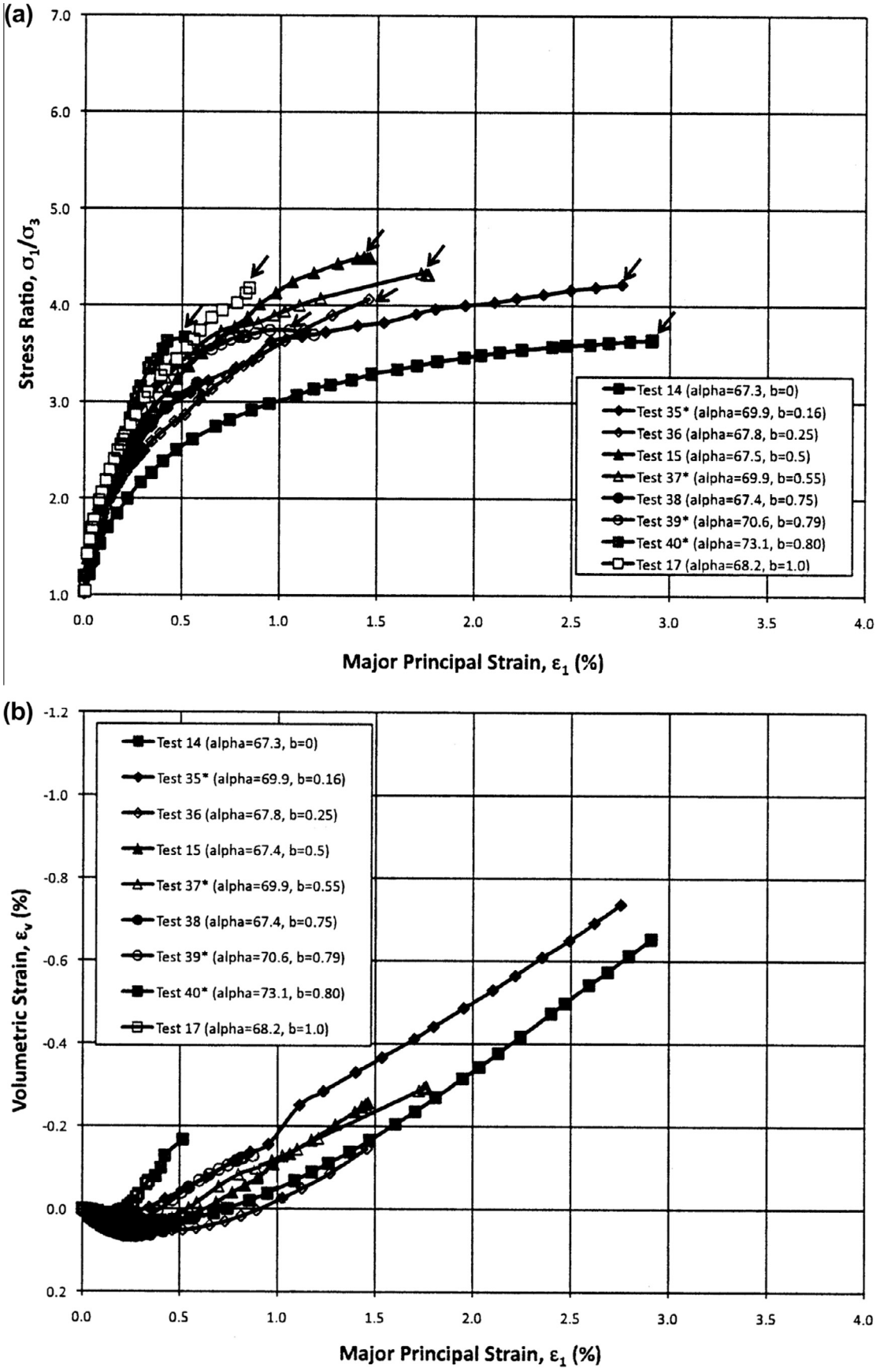

Fig. 6. (a) Stress–strain and (b) volume change relations for torsion shear test with $\alpha = 67.5°$ on hollow cylinder specimens of dense Nevada sand.

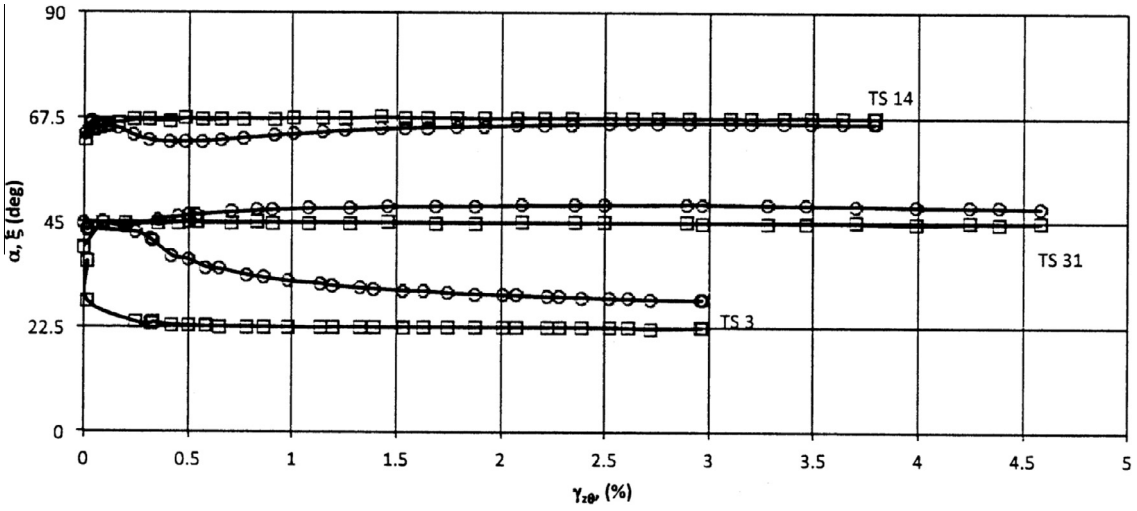

Fig. 7. Directions of principal strain increments (open circle) and stresses (open square) versus engineering shear strain for torsion shear tests with $b = 0.0$ on dense Nevada sand.

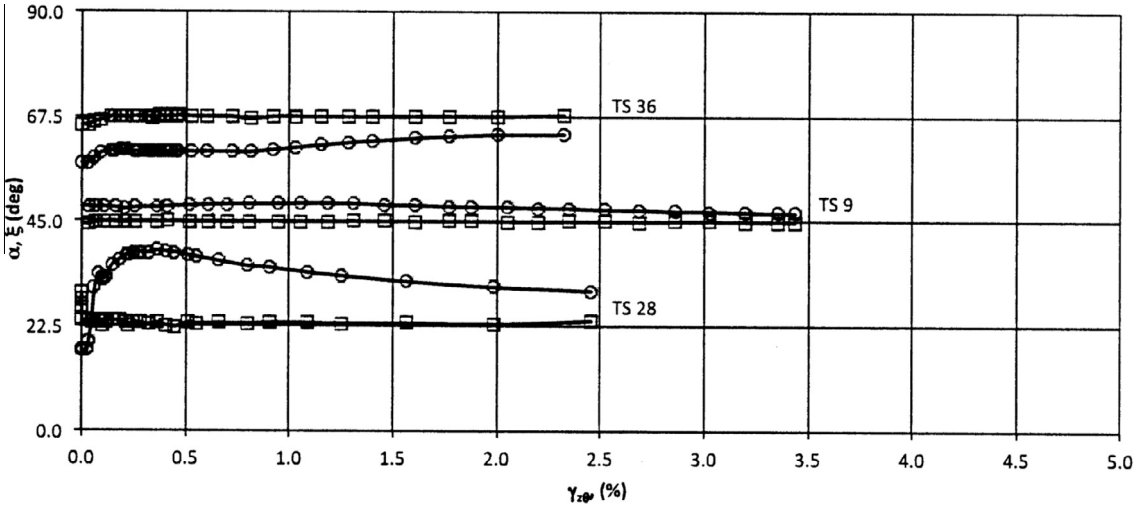

Fig. 8. Directions of principal strain increments (open circle) and stresses (open square) versus engineering shear strain for torsion shear tests with $b = 0.25$ on dense Nevada sand.

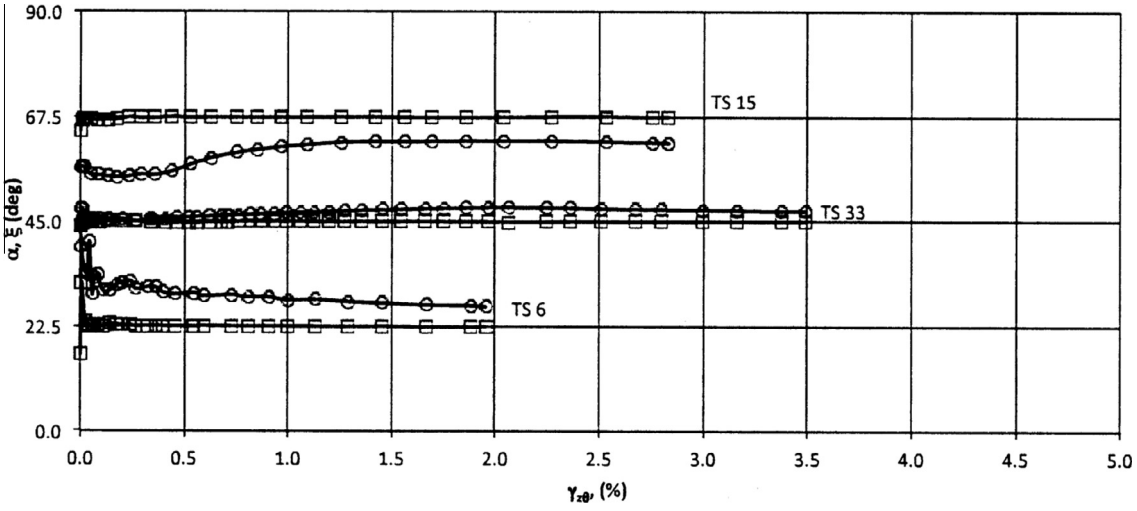

Fig. 9. Directions of principal strain increments (open circle) and stresses (open square) versus engineering shear strain for torsion shear tests with $b = 0.50$ on dense Nevada sand.

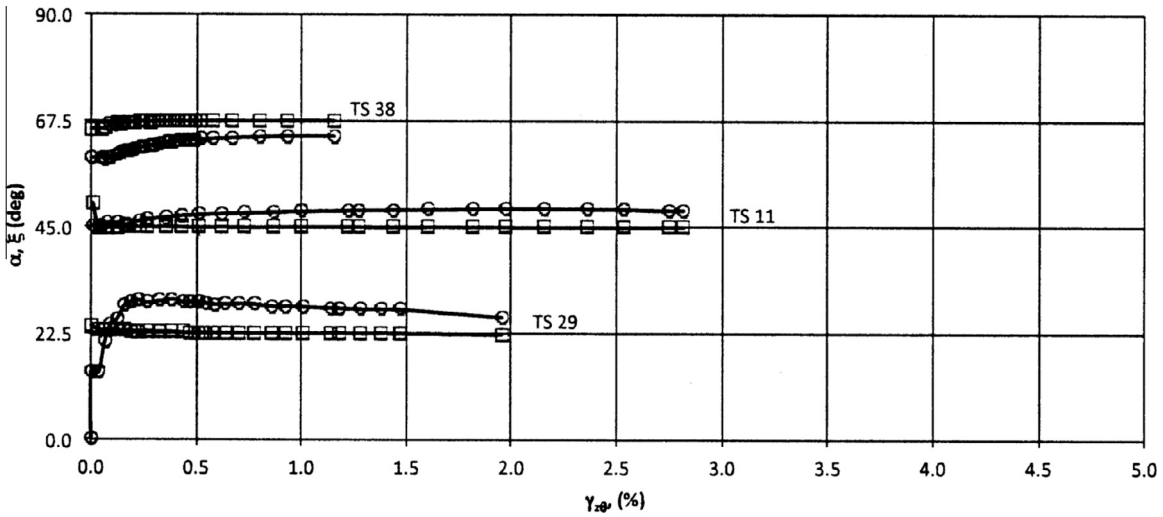

Fig. 10. Directions of principal strain increments (open circle) and stresses (open square) versus engineering shear strain for torsion shear tests with $b = 0.75$ on dense Nevada sand.

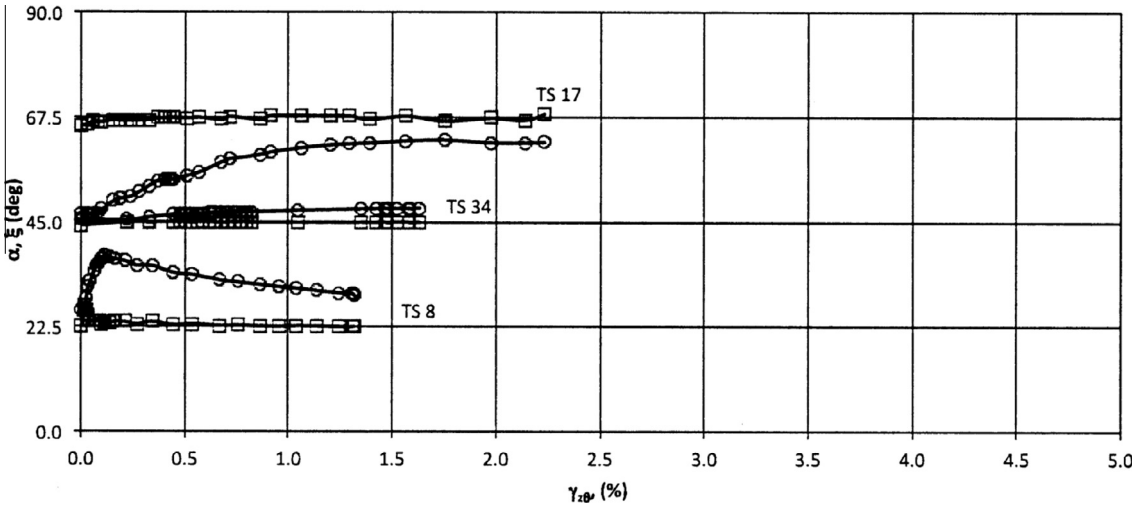

Fig. 11. Directions of principal strain increments (open circle) and stresses (open square) versus engineering shear strain for torsion shear tests with $b = 1.0$ on dense Nevada sand.

there does not appear to be any systematic variation with the value of $b = (\sigma_2 - \sigma_3)/(\sigma_1 - \sigma_3)$.

These deviations are caused by scatter similar to e.g. the scatter in strain-to-failure observed for repeated tests in triaxial compression. It is not caused by inaccuracy of the measurements, because the same instrumentation was used for all the experiments, and the errors due to experimental accuracy are small. Thus, it was estimated that the error on the α-values were in the order of 0.3°, and the error on the ξ-values were of similar magnitude. These are insufficient to invalidate the measurements and the conclusions presented here.

It is interesting to note that the major strain increment directions for $\alpha = 22.5°$, and $\alpha = 45°$ are slightly above the stress directions. For $\alpha = 67.5°$, the major principal strain increment directions are slightly below the major principal stress directions. This is due to the cross-anisotropic nature of the specimen in which the bedding planes are horizontal. At $\alpha = 22.5°$, the horizontal bedding planes cause the strain increment direction to become more horizontal and therefore show a slightly higher inclination than the σ_1-direction. At $\alpha = 45°$, this also occurs but to a lesser extent. However, at $\alpha = 67.5°$, the strain increment direction moves over to the other side of the principal stress direction. This pattern is observed for all b-values. Fig. 13 presents a schematic diagram showing the bedding planes of a specimen and the general pattern of directions of stress directions and strain increment directions for all b-values.

In nature, where the initial stress state is not isotropic but at a stress level closer to failure, the initial portions of the relations shown in Figs. 7–11 are not present. At higher stress levels (proximity to failure) the directions of major principal strain increments are controlled by the plastic strain components and the major principal strain increment directions are likely to be closer to the directions of major principal stress, but in general the two directions are not expected to coincide, even at failure. The deviations between the two directions are expected to follow the pattern indicated and discussed above.

It is clear from the experiments that the directions of the strain increment vectors do not coincide generally with the directions of the stress, i.e. the ξ- and the α-directions are generally non-coaxial. The pattern of behavior observed in these torsion shear experiments, which were performed with constant stress directions indicated by α, has to be modeled by a constitutive model that involves cross-anisotropic plastic hardening behavior.

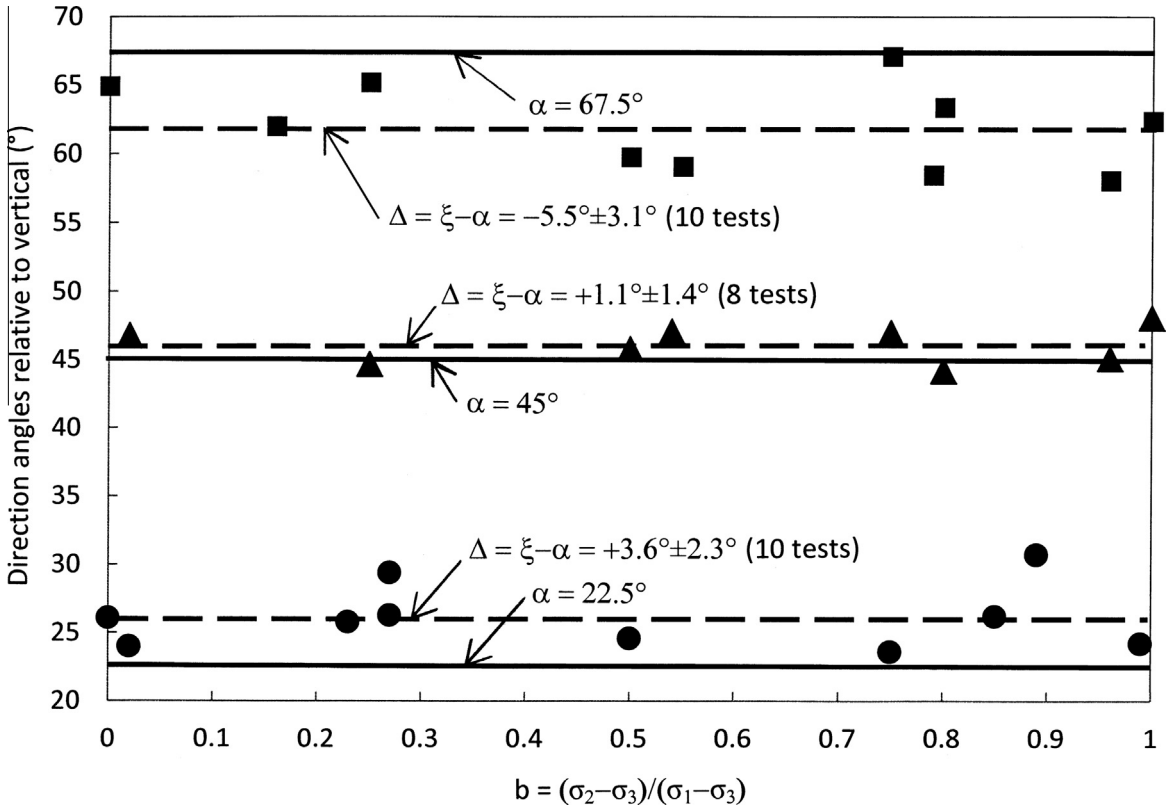

Fig. 12. Diagram of the deviations between major principal strain increment directions (ξ) and major principal stress directions (α) relative to vertical at failure.

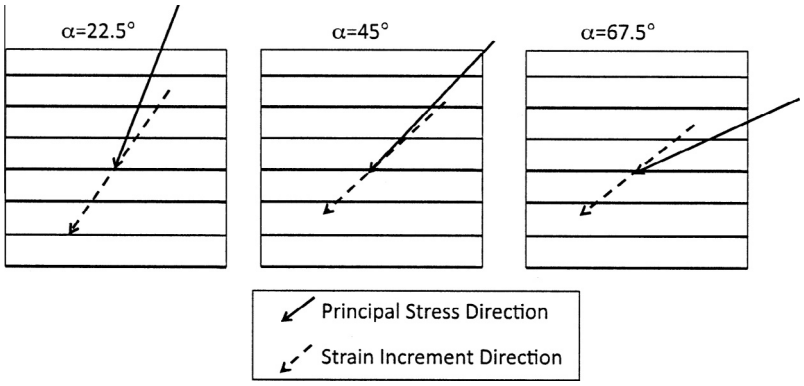

Fig. 13. Schematic patterns of principal strain increment directions and principal stress directions observed in torsion shear tests on dense Nevada sand.

6. Conclusion

The results of carefully performed torsions shear tests on hollow cylinder specimens of dense Nevada sand have been interpreted in terms of the directions in physical space of the major principal strain increments relative to the major principal stresses, which were maintained in constant directions during each test. The two directions were found to be generally non-coaxial, even at failure, which was manifested as development of shear bands. The average deviations between the two directions varied in a systematic manner between +3.6° and −5.5°, but a fair amount of scatter was observed in the experiments. To model this behavior, a constitutive model is required that includes effects of cross-anisotropy.

In a previous study (Lade et al., 2009) it was concluded that the directions of major principal strain increments essentially coincide with the directions of the major principal stress at the condition of failure. In that study the sand behaved as an isotropic material at failure, a surprising finding in view of the fact that the same torsion shear experiments showed considerable influence of cross-anisotropy on shear band orientations and on the shape of the failure surface. In those tests the stress paths were quite general with large variations in directions of major principal stress, and there might have been a tendency to oversimplify the conclusions from that study. In comparison, the present study employed constant directions of the major principal stress throughout the tests and the major principal strain increment directions therefore had a larger range of strains to establish themselves.

Acknowledgments

The research presented here was performed with support from the National Science Foundation under Grant No. CMMI-0757827. Grateful appreciation is expressed for this support.

References

Abelev, A.V., Lade, P.V., 2003. Effects of cross-anisotropy on three dimensional behavior of sand. I: stress–strain behavior and shear banding. ASCE J. Eng. Mech. 129 (2), 160–166.

Broms, B.B., Casbarian, A.O., 1965. Effects of rotation of the principal stress axes and of the intermediate principal stress on shear Strength. In: Proc. 6th Int. Conf. Soil Mech. Found. Eng., Montreal, Canada, vol. I, pp. 179–183.

Chaudhary, S.K., Kuwano, J., 2003. Anisotropic multiple yielding of dense Toyoura sand in p'-constant shear plane. Soils Found. 43 (4), 59–69.

Frydman, S., Talesnick, M., Puzrin, A., 1995. Colinearity of stresses, strains, and strain increments during shearing of soft clay. ASCE J. Geotech. Eng. 121 (2), 174–184.

Hicher, P.-Y., Lade, P.V., 1987. Rotation of principal directions in K_0-consolidated clay. ASCE J. Geotech. Eng. 113 (7), 774–788.

Hight, D.W., Gens, A., Symes, M.J., 1983. The development of a new hollow cylinder apparatus for investigating the effects of principal stress rotation in soils. Geotechnique 33 (4), 355–383.

Hong, W.P., Lade, P.V., 1989a. Elasto-plastic behavior of K_0-consolidated clay in torsion shear test. Soils Found. 29 (2), 57–70.

Hong, W.P., Lade, P.V., 1989b. Strain increment and stress directions in torsion shear tests. ASCE J. Geotech. Eng. Div. 115 (10), 1388–1401.

Ishihara, K., Towhata, I., 1983. Sand response to cyclic rotation of principal stress direction as induced by wave loads. Soils Found. 33 (4), 11–26.

Kuwano, R., Jardine, R.J., 2007. A triaxial investigation of kinematic yielding in sand. Geotechnique 57 (7), 563–579.

Lade, P.V., 1975. Torsion shear tests on cohesionless soil. In: Proc. 5th Panamerican Conf. Soil Mech. Found. Eng.. Buenos Aires, Argentina, pp. 117–127, I.

Lade, P.V., 1976. Interpretation of torsion shear tests on sand. In: Proc. 2nd Int. Conf. Numerical Meth. Geomech., Blacksburg, VA, vol. I, pp. 381–389.

Lade, P.V., 1981. Torsion shear apparatus for soil testing. In: Yong, R.N., Townsend, F.C. (Eds.), Laboratory Shear Strength of Soil, ASTM STP 740. ASTM, Philadelphia, Pa., pp. 145–163.

Lade, P.V., Abelev, A.V., 2005. Characterization of cross-anisotropic soil deposits from isotropic compression tests. Soils Found. 45 (5), 89–102.

Lade, P.V., Duncan, J.M., 1973. Cubical triaxial tests on cohesionless soil. ASCE J. Soil Mech. Found. Div. 99 (SM10), 793–812.

Lade, P.V., Kirkgard, M.M., 2000. Effects of stress rotation on cross-anisotropic behavior of natural K_0-consolidated soft clay. Soils Found. 40 (6), 93–105.

Lade, P.V., Nam, J., Hong, W.P., 2008. Shear banding and cross-anisotropic behavior observed in laboratory sand tests with stress rotation. Can. Geotech. J. 45 (1), 74–84.

Lade, P.V., Nam, J., Hong, W.P., 2009. Interpretation of strains in torsion shear tests. Comput. Geotech. 36 (1–2), 211–225.

Lade, P.V., Rodriguez, N.M., Van Dyck, E.J., 2013. Effects of principal stress directions on 3D failure conditions in cross-anisotropic sand. ASCE J. Geotech. Geoenvironm. Eng., in press.

Lade, P.V., Rodriguez, N.M., 2013. Comparison of true triaxial and hollow cylinder tests on cross-anisotropic sand specimens. ASTM Geotech. Test. J., submitted for publication.

Nishimura, S., Minh, N.A., Jardine, R.J., 2007. Shear strength anisotropy of natural London clay. Geotechnique 57 (1), 49–62.

Pradhan, B.S., Tatsuoka, F., Horii, N., 1988. Simple shear testing on sand in a torsional shear apparatus. Soils Found. 28 (2), 95–112.

Saada, A.S., Baah, A.K., 1967. Deformation and failure of a cross anisotropic clay under combined stresses. In: Proc. 3rd Panamerican Conf. Soil Mech. Found. Eng., I. Caracas, Venezuela, pp. 67–88.

Saada, A.S., Bianchini, G.F., Liang, L., 1994. Cracks, bifurcation, and shear bands propagation in saturated clays. Geotechnique 44 (1), 35–64.

Saada, A.S., Liang, L., Figueroa, J.L., Cope, C.T., 1999. Bifurcation and shear band propagation in sands. Geotechnique 49 (3), 367–385.

Sayao, A., Vaid, Y.P., 1991. A critical assessment of stress nonuniformities in hollow cylinder test specimens. Soils Found. 31 (1), 60–72.

Shibuya, S., Hight, D.W., Jardine, R.J., 2003. Local boundary surfaces of a loose sand dependent on consolidation path. Soils Found. 43 (3), 85–93.

Sivathayalan, S., Vaid, Y.P., 2002. Influence of generalized initial state and principal stress rotation on the undrained response of sands. Can. Geotech. J. 39 (1), 63–76.

Symes, M.J.P.R., Gens, A., Hight, D.W., 1984. Undrained anisotropy and principal stress rotation in saturated sand. Geotechnique 34 (1), 11–27.

Symes, M.J.P.R., Gens, A., Hight, D.W., 1988. Drained principal stress rotation in saturated sand. Geotechnique 38 (1), 59–81.

Tatsuoka, F., Sonoda, S., Hara, K., Fukushima, S., Pradhan, T.B.S., 1986. Failure and deformation of sand in torsional shear. Soils Found. 26 (4), 79–97.

Vaid, Y.P., Sayao, A., 1995. Proportional loading behaviour of sand under multiaxial stresses. Soils Found. 35 (3), 23–29.

Vaid, Y.P., Sayao, A.S.F., Hou, E., Negussey, D., 1990. Generalized stress path dependent soil behaviour with a new hollow cylinder torsional apparatus. Can. Geotech. J. 27 (5), 601–616.

Wang, Q., Lade, P.V., 2001. Shear banding in true triaxial tests and its effect on failure in sand. ASCE J. Eng. Mech. 127 (8), 754–761.

Yang, Z.X., Li, X.S., Yang, J., 2007. Undrained anisotropy and rotational shear in granular materials. Geotechnique 57 (4), 371–384.

Zdravkovic, L., Jardine, R.J., 2000. Undrained anisotropy of K_0-consolidated silt. Can. Geotech. J. 37 (1), 178–200.